Synthesis and characterization of the Mars-relevant phosphate minerals Fe- and Mg-whitlockite and merrillite and a possible mechanism that maintains charge balance during whitlockite to merrillite transformation

REVISION 1

Christopher T. Adcock[1]*, Elisabeth M. Hausrath[1], Paul M. Forster[2,3], Oliver Tschauner[1,3] and Kirellos J. Sefein[1†]
Corresponding author email: adcockc2@unlv.nevada.edu

[1]Department of Geoscience, University of Nevada Las Vegas, 4505 S. Maryland Pkwy., Las Vegas, NV 89154
[2]Department of Chemistry, University of Nevada Las Vegas, 4505 S. Maryland Pkwy., Las Vegas, NV 89154
[3]HiPSEC, University of Nevada Las Vegas, 4505 S. Maryland Pkwy., Las Vegas, NV 89154
[†]Current address: ConocoPhillips School of Geology and Geophysics, University of Oklahoma, 660 Parrington Oval., Norman, OK 73019

Abstract

Merrillite [$Ca_9NaMg(PO_4)_7$] occurs as a dominant primary Ca-phosphate mineral in martian meteorites and therefore presumably also on Mars. The mineral is an important phase in exploring differences in geologic processes between Earth and Mars, and also has astrobiological implications due to its potential role as a significant source of the bio-essential nutrient phosphate. Merrillite does not occur terrestrially as a discrete mineral phase, making it difficult to obtain for Mars-relevant studies. It can, however, be synthesized from a similar terrestrial mineral, whitlockite (natural or synthetic), through dehydrogenation. Here we present methods for synthesizing relatively large quantities (0.5 g or greater per batch) of coarse crystalline (75 μm+) Mg-whitlockite, Fe-whitlockite, mixed Fe/Mg-whitlockites, and from these synthesized minerals produce Mg-merrillite, ferrous and ferric Fe-merrillite and ferrous and ferric mixed Fe/Mg-merrillite. Chemistry and atomic structures of synthesized Fe- and mixed Fe/Mg-whitlockite and ferrous and ferric Fe- and mixed Fe/Mg- merrillite resulting from single-crystal X-ray diffraction, infra-red spectroscopy, and electron microprobe analyses are presented. We also present a mechanism for maintaining charge balance during the formation of merrillite from

whitlockite. Our results shed light on these mineral structures for future martian studies, and provide methods for creating coarse crystalline merrillite for use in Mars-relevant thermodynamic, kinetic, soil/dust simulant, crystallographic, astrobiological, and other studies.

Keywords: Whitlockite, merrillite, Mg, Fe, structures, synthesis, dehydrogenation, phosphate, Mars, astrobiology.

Introduction

Merrillite is an anhydrous calcium phosphate mineral that occurs in lunar samples and meteorites, including martian meteorites (Jolliff et al., 1993; McSween et al., 1996; Xie et al., 2002; Terada et al., 2003). The IMA formula for merrillite is $Ca_9NaMg(PO_4)_7$, though merrillite can also be iron-bearing (Jolliff et al., 2006). Synthetic merrillite also lacks Na^+ and charge balance is maintained by additional Ca^{2+} [i.e. $Ca_{9.5}Mg(PO_4)_7$] . Merrillite is of particular interest to martian studies because it is the dominant primary phosphate mineral in martian meteorites (McSween et al., 1996; McSween and Treiman, 1998), and thus presumably also on Mars. This is in contrast to Earth where fluorapatite [$Ca_5(PO_4)_3F$] is the dominant terrestrial primary phosphate mineral and the nearest analog to merrillite, the mineral whitlockite [$Ca_9Mg(PO_3OH)(PO_4)_6$], occurs as a component of teeth and bones in vertebrates, but outside of biological systems is a rare alteration product of phosphate pegmatites. Merrillite is also the major carrier of Rare Earth Elements (REE) in martian meteorites (McSween et al., 1996; McSween and Treiman, 1998; Shearer et al., 2011a) and likely one of the major sources of the phosphorus observed in phosphorus rich martian soils and dust (Goetz et al., 2005; Greenwood and Blake, 2006; Brückner et al., 2008). Phosphate minerals such as merrillite and apatite are

thought to react in late stage martian magmas (McCubbin and Nekvasil, 2008; Filiberto and Treiman, 2009; Gross et al., 2013b), and their presence and intergrowth relationships with each other within martian rocks (or meteorites) can be useful indicators of crystallization and melt evolution, including the evolution of both water and halogen budgets over time (Patiño Douce and Roden, 2006; Patiño Douce et al., 2011; Gross et al., 2013a; Gross et al., 2013b). Such use of merrillite/apatite intergrowth relationships may also be applicable to other differentiated bodies outside of Mars (Shearer et al., 2011b). Phosphate minerals have also been shown to be altered in acid vapor environments, potentially recording important characteristics of the reacting environment (Lane et al., 2008; Hausrath et al., 2013; Hausrath and Tschauner, 2013). In addition, phosphate is a required component in fundamental biologic reactions as well as considered critical to reactions that may have led to life on Earth (Gulick, 1955; Westheimer, 1987; Schwartz, 2006). The alteration of phosphate minerals such as merrillite has important implications for phosphate availability and the potential for martian abiogenesis and development of life on that planet (Adcock et al., 2013). Thus merrillite is an important phase in exploring the differences in petrogenesis, mantle evolution, surface processes and other geologic processes between Earth, Mars and possibly other bodies (McSween et al., 1996; Treiman, 2003; Shearer et al., 2011a).

The importance of merrillite in martian processes makes a readily available source of the mineral desirable for laboratory study. However, single-phase natural merrillite only occurs in extraterrestrial materials and thus studies requiring merrillite must obtain the mineral directly from meteorites or lunar samples, or through synthesis. Here we present methods for producing fairly large quantities of crystalline Fe/Mg-bearing merrillite for use in Mars-relevant studies, the

chemistry and atomic arrangements of the synthetic minerals, and a proposed mechanism for maintaining charge balance during the formation of merrillite from whitlockite.

Background

Merrillite was first described in meteorites by Merrill (1915; 1917). Wherry (1917) was the first to suggest applying "merrillite" as the name of the extraterrestrial mineral. Merrillite is chemically and structurally similar to the terrestrially occurring mineral whitlockite; in fact, though merrillite is not found terrestrially as a discrete mineral phase outside of biological systems, it does occur as a minor component within whitlockite, with which it forms a solid solution (Hughes et al., 2008). In biological systems, merrillite forms in dental calculi and urinary stones (Dorozhkin and Epple, 2002). The similarities of merrillite and whitlockite have resulted in overlapping use of the mineral names within the literature, though they are not strictly the same mineral. Whitlockite was first described by Frondel (1941) as a late stage calcium phosphate mineral associated with pegmatites. Frondel and Prien (1946) later applied the term "whitlockite" to synthetic tricalcium phosphate [β-$Ca_3(PO_4)_2$ or commonly β-TCP] because of chemical and structural similarities of that phase. The similarity of merrillite, whitlockite, and β-TCP led Fuchs (1962) to argue, based primarily on powder X-ray diffraction data, that the three phases were the same and that the term "merrillite" should be abandoned in favor of "whitlockite". Subsequent research conclusively demonstrated that merrillite and β-TCP, while isostructural and very similar to whitlockite, are distinct, and lack the required hydrogen of whitlockite (Gopal and Calvo, 1972; Dowty, 1977; Rubin, 1997; Hughes et al., 2008). Dowty (1977) suggested "merrillite" as the more appropriate name for the hydrogen-free form found in meteorites. However, because of the historical usage of "whitlockite" and the difficulty of

confirming the hydrous or anhydrous nature of the phases, the term "whitlockite" continues to be occasionally used synonymously or interchangeably when describing merrillite (e.g. Ruszala and Kostiner, 1980; Jolliff et al., 1993; McSween et al., 1996; Terada et al., 2003; Orlova et al., 2009). This is especially the case in biomedical fields where synthetic merrillite compounds, such as β-TCP, are important in bio-ceramics and are often referred to as whitlockite or β-whitlockite (e.g. Jarcho et al., 1979; Lagier and Baud, 2003). In this paper, as in some other studies that discuss both merrillite and whitlockite (e.g. Hughes et al., 2006; Jolliff et al., 2006) the term "merrillite" is used to describe the anhydrous extraterrestrial (and synthetic) Ca-phosphate mineral, and the term "whitlockite" to refer to the hydrogenated terrestrial mineral form.

The most common method of synthesizing merrillite powder is solid state sintering, which involves heating relevant powdered calcium phosphate chemistry to >1025 °C. The method typically requires several cycles of regrinding the material during the synthesis process (e.g. Lazoryak et al., 1996; Belik et al., 2002; Orlova et al., 2009), and therefore produces a very fine powder. This general method is used to produce commercially available β-TCP powders and ceramics, synthetic Ca-endmember merrillite materials. The same methods have been used to synthesize other types of merrillite powders (Teterskii et al., 2007; Orlova et al., 2009), including Mg-merrillite and ferric Fe-merrillite (Lazoryak et al., 1996). A drawback to this general method is that it produces only very fine powders, which may not be preferred for some studies (e.g. dissolution kinetics, crystallography, soil simulants). The commercial version is also an endmember lacking in Fe or Mg and thus chemically dissimilar to the merrillite commonly found in lunar samples or martian meteorites (Jolliff et al., 2006).

Another method of synthesizing merrillite is through the heating of whitlockite to >1000 °C for at least 24 hours to drive off the "essential hydrogen" (Gopal and Calvo, 1972; Hughes et al., 2008). This method has the advantage of being simple to perform and has been applied to both synthetic Mg-whitlockite and natural whitlockite crystals to produce crystalline merrillite rather than powders. However, natural terrestrial whitlockite is itself uncommon and generally restricted to small quantities associated with pegmatites. Thus, in order to synthesize quantities of high purity crystalline Mg- and Fe-merrillite for use in Mars-related kinetic, thermodynamic, astrobiological, or other studies, the synthesis of Mg- and Fe-whitlockite in large quantity is required.

Whitlockite can be synthesized by the Rowles method (Rowles, 1968) which involves hydrolysis of brushite in magnesium chloride solution to create Mg-whitlockite. The method can create pure Mg-whitlockite crystalline material and large output masses (500+ g). The crystalline material generated by this method is very fine with specific surface areas (SSA) of 3-7 m^2/g (geometrically equivalent to 0.3-0.6 μm diameter average particle size)(Hamad and Heughebaert, 1986) making it of limited usefulness in kinetic, simulant, crystallographic, or other studies where coarser crystalline material is preferred. Hydrothermal methods, however, can create coarser crystalline material. Gopal et al. (1974) synthesized coarse, up to 500 μm per side, crystalline Mg-whitlockite using such a method. The method required the pre-synthesis and processing of a calcium phosphate gel and a large (6mm x 100mm) single-use gold tube to contain the reagents during heating to 300 °C, making it less practical for synthesizing in quantity. Hughes et al. (2008) inadvertently produced a small amount (i.e. "a few crystals") of Mg-whitlockite by similar methods while hydrothermally recrystallizing hydroxyapatite [$Ca_5(PO_4)_3OH$]. Their method involved first synthesizing hydroxyapatite powder from a calcium

147 phosphate solution and suspending it in 10ml of distilled water with the pH adjusted to 2.79
148 using phosphoric acid. The resulting suspension was sealed in a reusable 23ml Teflon lined acid
149 digestion vessel and heated to 240 °C for 5 days. The output mass from the hydrothermal
150 treatment consisted mainly of elongate, recrystallized hydroxyapatite along with a small number
151 of large, well-formed, Mg-whitlockite crystals. The apparent cause of whitlockite synthesis was
152 Mg contamination from an undetermined source. Here we present methods based on Hughes et
153 al. (2008) to generate large quantities of single phase Mg-whitlockite and, from that whitlockite,
154 Mg-merrillite by intentionally supplying Mg^{2+} to the synthesis. We also developed methods to
155 generate large amounts of crystalline Fe-whitlockite, as well as mixed Fe/Mg-whitlockites, and
156 ferrous, ferric, and mixed Fe/Mg-merrillites. Atomic parameters are presented for ferrous, ferric,
157 and mixed merrillite and Fe- and mixed whitlockite, as well as a proposed mechanism for
158 maintaining charge balance during the formation of merrillite from whitlockite.
159

160 ## Methods

161 ### Whitlockite synthesis

162 Based on preliminary experiments (deposit items Appendix A and Table A1[1]), the
163 following synthesis methods were developed for Mg- and Fe-whitlockite production: a solution
164 containing 90ml of high purity (18.2 MΩ) water, laboratory grade hydroxyapatite (Spectrum,
165 reagent grade), and either magnesium nitrate hexahydrate for Mg-whitlockite (J.T. Baker, ACS
166 grade) or troilite for Fe-whitlockite (Alfa Aesar, Fe[II]S 99%) were combined in a 125ml Parr
167 acid digestion vessel (Parr #4748) with an acid washed Teflon liner. Specific volumes and
168 masses are contained in Table 1. Once the solution was mixed, it was acidified to pH <2.8 with

[1] Deposit items are available two ways: For a paper copy contact the Business Office of the Mineralogical Society of America (see inside front cover of recent issue) for price information. For an electronic copy visit the MSA web site at http://www.minsocam.org, go to the American Mineralogist Contents, find the table of contents for the specific volume/issue wanted, and then click on the deposit link there.

concentrated phosphoric acid (Alfa Aesar, ACS grade). The vessel was then sealed and incubated in an oven at 240 °C for 7 days. At the end of 7 days, the vessel was removed from the oven and quenched in a water bath in an effort to prevent any further reaction. After cooling, the vessel was opened and the solution decanted leaving the solids. Solid material was rinsed from the vessel using ethanol, allowed to air dry for 24 hours, weighed, and inspected by optical microscopy for preliminary phase identification. Impurities, first determined by powder XRD and then optically by morphology thereafter, were typically hydroxyapatite, monetite ($CaHPO_4$). In the case of Fe-bearing whitlockite, additional opaque materials presumed to be Fe-phases occurred in quantities too minor for powder XRD analysis. These impurities were primarily confined to the <75 μm fraction and output masses were brush sieved on 200 mesh screen to remove that size fraction. Crystals were confirmed as Mg- or Fe-whitlockite by Scanning Electron Microscopy (SEM) with Energy Dispersive Spectroscopy (EDS), Electron Microprobe Analysis (EMP), Powder X-ray Diffraction (XRD), and Single Crystal X-ray Diffraction (SC-XRD).

Based on results from endmember experiments described above, mixed Fe/Mg-whitlockites were also successfully synthesized by combining both troilite and magnesium nitrate hexahydrate (J.T. Baker ACS grade, and Alfa Aesar Fe[II]S 99%, respectively) in the solution used within a single synthesis experiment. Table 1 contains the specific masses and volumes used to produce the mixed Fe/Mg-whitlockite that was further characterized in this study and it includes sodium (as NaCl) as part of the solution. Subsequent experiments indicated that the addition of NaCl in this method has no observable effect and can be omitted (see Results and Discussion and deposit items Appendix A and Table A1), but it is included in Table 1 as this was the material further characterized in this study. Outside of solution chemistry, all other

parameters used in mixed Fe/Mg-whitlockite synthesis were the same as for the endmember whitlockite synthesis (e.g. temperature, acidity, incubation time). Impurities found in mixed Fe/Mg synthesis batches (typically large polycrystalline aggregates, hydroxyapatite and opaque phases as determined optically) were primarily confined to the <75 μm and >150 μm fractions and output masses were brush sieved to isolate the 75-150 μm size fraction. Remaining crystalline material was confirmed as Fe/Mg-whitlockite by EMP and SC-XRD.

Merrillite synthesis

Merrillite can be synthesized from whitlockite (natural or synthetic) by dehydrogenation through heating to >1000 °C for at least 24 hours (Gopal et al., 1974; Hughes et al., 2008). In this study, crystalline Mg-merrillite was synthesized from synthetic Mg-whitlockite by heating to 1055 °C (+/-5 °C) for a minimum of 24 hours in a loosely covered 10 ml Pt crucible nested within a larger (100ml) alumina crucible for easier handling. After heating, the crucibles were removed and allowed to air cool. After cooling, resulting materials, typically white to clear in color, were removed from the crucible using a synthetic brush.

Crystalline ferric Fe-merrillite was synthesized in an identical manner as the Mg-merrillite described above, in a Pt crucible in ambient atmosphere. The process produces an orange/red colored material. Ferrous Fe-merrillite was synthesized in an evacuated (10^{-3} Torr) sealed SiO_2 tube in place of the Pt crucible to inhibit oxidation of Fe from ferrous to ferric in the Fe-whitlockite. Tubes were purged with argon three times to remove oxygen before final evacuation and sealing. SiO_2 glass wool (average 4 μm diameter) was used to prevent the loss of material from the tubes during purge and evacuation cycles. Whitlockite heat treated in this manner ranged in color from white/translucent to black and nearly opaque.

Mixed Fe/Mg-merrillite was synthesized both in a 10 ml Pt crucible in ambient atmosphere, and also in a triple argon purged evacuated (10^{-3} Torr) sealed SiO_2 tube to inhibit oxidation of the Fe in the Mg-Fe whitlockite, both as described above. Resulting materials from all merrillite syntheses were analyzed by optical microscopy, EMP and SC-XRD to confirm the phases. Oxidation of Fe during merrillite synthesis can mask detection of dehydrogenation by SC-XRD, so Fe-containing phases were additionally analyzed by Infrared Spectroscopy (IR). As with the Fe-endmember whitlockite treated in the same manner, the output material ranged in color from white/translucent to black and nearly opaque.

Analytical methods

Powder X-ray Diffraction (XRD) analyses were performed in the UNLV Geoscience XXL facility. Samples of synthesized Mg- and Fe-whitlockite, as well as impurities from synthesis, were powdered by hand in an agate mortar and pestle and subjected to powder XRD in a Panalytical X'pert Pro diffractometer using Cu Kα radiation. Scans were run at 45Kv and 40mA from 5-75° 2θ in continuous mode with step-size of 0.0084° and scan rate of 0.06° sec^{-1}. Patterns were identified and confirmed using Panalytical's X'pert Pro High Score Plus software.

Optical microscopy was used to identify synthesized phases based on crystal habit/morphology and previous XRD analyses. These identifications were carried out with a Barska tri-ocular stereomicroscope with a magnification range of 7x to 45x. An adaptor mounted Canon XTi camera was used for all optical photomicrographs.

Scanning Electron Microscopy (SEM) in secondary electron imaging mode (SEI) and Energy Dispersive Spectrometry (EDS) was carried out on a JEOL 5600 SEM at the UNLV Electron Microanalysis and Imaging Laboratory (EMiL). Operating conditions were 20 KeV

and a 20 mm working distance. Analyses by Electron Microprobe (EMP) wavelength dispersive spectroscopy (WDS) were carried out in a JEOL JXA-8900 at the UNLV EMiL facility on polished epoxy mounts. Analysis conditions were 20 KeV and 10 nA using a 10 μm beam. Analyses were standardized using Smithsonian mineral standards of olivine (Mg, Fe) and apatite (Ca, P)(Jarosewich, 2002), and Harvard (Amelia) albite (Na)(McGuire et al., 1992).

Single Crystal X-ray Diffraction (SC-XRD) analyses were carried out using a Bruker APEXII single crystal diffractometer. An appropriate crystal was selected under paratone oil on a polarizing microscope and attached to a Kapton mount. A full sphere of data was collected with the sample cooled to 100 K using an Oxford nitrogen cryostream. An absorption correction utilized the Bruker software SADABS, structure solution was performed using a beta-version of SHELXT, and refinement was carried out using a combination of SHELX (Sheldrick, 2007) and OLEXII (Dolomanov et al., 2009). Bond valence calculations from SC-XRD data were conducted using VALIST (Wills, 1999).

Infrared (IR) spectra were obtained with a Digilab FTS 7000 series FT-infrared spectrometer on powdered samples using a photo-acoustic chamber attachment. Analyses were performed under ambient conditions at 2.5 KHz and a resolution of 8 cm^{-1} for 64 total scans. Data were collected over the range of 400 to 4000 cm^{-1}. Carbon black was used to obtain a background versus subsequent spectra.

Synchrotron X-ray diffraction experiments were conducted on two samples (a red ferric Fe/Mg-merrillite crystal and a dark colored ferrous Fe/Mg-merrillite crystal) at the superconducting bending magnet beamline 12.2.2 at the Advanced Light Source (ALS), Lawrence Berkeley National Laboratory, with the goal of identifying any trace fine-grained phases within the merrillite. Primary beam energy was 20.000 keV and a MAR345 image plate

detector was utilized. Detector parameters were calibrated and corrected for geometric distortions based on a LaB6 NIST powder diffraction standard using the Fit2D software (Hammersley et al., 1996). The X-ray beam at beamline 12.2.2 of the ALS is focused by Kirkpatrick-Baesz mirrors vertically and horizontally to 10 x 15 μm^2. Crystal samples were mounted on the tips of quartz glass fibers of 30 μm diameter and centered on the phi rotation axis. Exposures were taken over 160 s while the samples were oscillated by +/-40 degrees around the phi axis. Recorded images were integrated using Fit2D (Hammersley et al., 1996). We first used Fit2D to mask strong reflections from merrillite and any remaining minor untransformed whitlockite in the diffraction image frames and integrated the remaining patterns. Integrated patterns were still dominated by merrillite reflections and less intense whitlockite reflections. The contributions from both these phases were fitted by a Le Bail refinement (Le Bail, 2005). Remaining reflections were then identifiable as fine-grained inclusions. We used the first strong diffraction peaks of these fine-grained inclusions for a search in the American Mineralogist database (Downs and Hall-Wallace, 2003) and commercial data bases (ICSD) for identifying possible inclusion phases (Bergerhoff and Brown, 1987).

Results and Discussion

Optimization of Whitlockite Synthesis

Results of preliminary Mg-whitlockite experiments indicated that the concentration of solids in solution (g/L) was a strong control on Mg-whitlockite formation (Table A1 and Appendix A, on deposit[1]). Concentrations of greater than approximately 22 g/L produced primarily monetite ($CaHPO_4$) and hydroxyapatite (HAP) crystalline material rather than whitlockite. Concentrations of less than 22 g/L, including the 14.5 g/L used in the finalized

method, produced yields consisting primarily of well formed crystals of Mg-whitlockite confirmed by morphology, SEM EDS, powder XRD, and SC-XRD (Figures 1A and 2A). Solution concentrations of significantly less than 14.5 g/L (e.g. 11.1 g/L) produced whitlockite, but in smaller amounts (Table A1, on deposit[1]). Variations in incubation time (5-14 days) indicated that most crystal growth occurred in the first 7 to 8 days. Longer incubation times (up to 14 days) did not produce significantly larger crystals. Variations in pH from 2.1 to 2.8 did not appear to have any significant effect. Scaling up from 23ml vessels to 125ml vessels had no effect as long as solution concentrations were maintained. Temperature (i.e. 240 °C) was not varied and represented the highest safe temperature rated for the vessels used. The ratio of HAP to magnesium nitrate hexahydrate (3.33: 1) was not varied significantly, but minor changes (2.93:1 to 3.52:1) had no noticeable effect on syntheses. Overall yields from multiple batches of Mg-whitlockite synthesis using the final method had an average yield of >700 mg (Figs. 1A and 2A, deposit item Table A1). The <75μm fraction was removed to minimize impurities (i.e. monetite and hydroxyapatite); this fraction averaged <2% of the total output mass. Imperfections within some crystals, mainly in the larger size fraction, were apparent optically, but centralized clusters of inclusions similar to those seen by Hughes at al. (2008), while present, were uncommon. Most crystals (>80%) were over 150 μm and the largest crystals were 2mm. Polycrystalline aggregates of whitlockite occurred in the >75 μm fraction but the majority of the material were single crystals. EMP analyses of synthesized crystals (Table 2) confirmed Mg-whitlockite stoichiometry as $Ca_{9.0}Mg_{0.9}(PO_3OH)(PO_4)_6$.

Attempts to synthesize Fe-whitlockite using $FeCl_2$ as the source of Fe failed to produce the mineral in amounts detectable by optical microscopy, even at total solid in solution concentrations as low as 12.0 g/L. Instead, crystal morphologies consistent with monetite and

recrystallized HAP were produced as well as minor opaques (presumably Fe phases). The subsequent use of Fe(II)S as the source of Fe did produce Fe-whitlockite. Aggregate and hydroxyapatite production were minimized by decreasing the concentration of solids in solution from an initial 16.1 g/L to < 12.0 g/L. To minimize iron sulfide phases, the ratio of hydroxyapatite to Fe(II)S in solution was increased from ~9:1 (near stoichiometric ideal) to between 16:1 and 20:1 in an effort to "starve" the system of Fe. Yields from Fe-whitlockite syntheses using the final method described in the methods section averaged >500 mg of largely well formed whitlockite crystals (Figs. 1B and 2B, deposit item Table A1). Impurities (i.e. iron sulfides, hydroxyapatite, and monetite) mainly occurred in the <75 μm fraction which could be removed through sieving. The <75 μm fraction accounted for 33% of the total output mass on average. Inter-crystalline Fe-films were apparent optically in some aggregates (Fig. 1C). Some Fe-whitlockite crystals themselves contained minor intra-crystalline Fe-film deposits (determined optically) on earlier growth surfaces (Fig. 1B), with the crystals separable by picking. Minor amounts of Mg (0.14 wt. % as MgO) were also detected in Fe-whitlockites by EMP (Table 2). Like Hughes et al. (2008), the source of Mg is unknown, but is most likely from trace impurities in the reagents used. EMP analyses of synthesized crystals (Table 2) confirmed synthetic Fe-whitlockite stoichiometry as $Ca_{9.0}Fe_{1.0}(P_{1.0}O_3OH)(PO_4)_6$.

While Mg- and Fe-endmember whitlockite (and the merrillite synthesized from them) represent closer analogs to naturally occurring minerals than a phase like β-$Ca_3(PO_4)_2$, mixed Fe/Mg phases are closer analogs still. Two early experiments to produce mixed Fe/Mg-whitlockite failed to produce any significant whitlockite (Table A1 on deposit[1]). With understanding gained from further endmember experiments, another set of experimental conditions was tested with a lower solution concentration (13.0 g/L as opposed to >17 g/L for the

earlier attempts). This experiment included a source of Na^+ as part of the solution (included in the solution concentration noted above). Though Na^+ does not generally occur in whitlockite, the ion does occur in a specific Ca^{2+} site in natural merrillite, including merrillite found in martian meteorites where Na^+ content can be as high as 2 wt.% (Jolliff et al., 2006). The batch produced Fe/Mg mixed whitlockite (Figs. 1D and 2C) along with impurities of hydroxyapatite and monetite, and large (>150 μm) polycrystalline aggregates. Most impurities were in the >150 μm and <75 μm size fractions, leaving the 75-150 μm size fraction the purest. This fraction comprised 39% of the total output mass. EMP analyses showed no incorporation of Na^+ into any of the synthesized material and an average stoichiometry of $Ca_{9.0}Fe_{0.7}Mg_{0.3}(PO_3OH)(PO_4)_6$ (Table 2). The whitlockite seems to preferentially incorporate Mg, as the whitlockite from this batch had a Fe to Mg molar ratio of ~7:3 but the molar ratio of Fe to Mg in the reactants added was ~9:3. EMP analyses of results from additional mixed Fe/Mg-whitlockite synthesis experiments support this observation (Table A2, on deposit). It is also of note that the mixed Fe/Mg-whitlockite synthesis experiments had a higher failure rate than those of the endmembers, even after finding a generally successful set of conditions. Further investigation might yield the source of the failures or better refine the method. The lack of Na^+ incorporated within the whitlockite synthesized in these experiments suggests it may not be possible to incorporate the ion into the structure under hydrothermal conditions. Thus, mixed Fe/Mg-merrillite subsequently synthesized from the mixed Fe/Mg-whitlockite would also lack the sodium generally found in martian and lunar merrillite. Further investigation to determine conditions that favor Na^+ substitution in merrillite are warranted as they could potentially reveal important information about the specific martian environments in which merrillite forms. Nevertheless, sodium-free mixed Fe/Mg-bearing merrillite represents a better analog to martian merrillite than

pure endmember phases. EMP analyses revealed standard deviations of Fe and Mg contents were slightly higher than those of endmember synthesized material (Table 2). However, the minor increase in inhomogeneity should not limit the usefulness of the material for most studies.

Merrillite Synthesis

Merrillite and whitlockite structures are too similar to be easily distinguished by powder XRD, thus heat-treated materials were analyzed by SC-XRD and EMP to determine if the whitlockite to merrillite transformation had occurred. In the case of Mg-merrillite, SC-XRD (discussed in more detail below under Crystallography) confirmed synthesis had occurred and EMP analyses of the resulting Mg-merrillite (Table 2) indicated a stoichiometry of $Ca_{9.4}Mg_{1.1}(PO_4)_{7.0}$, compared to $Ca_{9.0}Mg_{0.9}(PO_3OH)(PO_4)_6$ of the starting Mg-whitlockite. The higher stoichiometric value for Ca^{2+} results from Ca substitution for charge balance due to dehydrogenation. Dehydrogenation is also the likely cause of higher observed totals for EMP analyses of Mg-merrillite versus the Mg-whitlockite used to synthesize it (99.35% versus 98.02% respectively). The synthesized Mg-merrillite maintained the crystallinity and morphology of the starting whitlockite material (Fig. 1E).

Fe-merrillite synthesis proved more complex than Mg-merrillite synthesis due to the apparent oxidation of ferrous Fe^{2+} to ferric Fe^{3+} when heated in open air. Fe-whitlockite samples heat-treated in open air (i.e. in the Pt crucible) changed color from white to orange or yellow. Like the Mg-merrillite, EMP analyses of the heat treated material showed overall totals rise from 98.15% for the original whitlockite to 98.80% for the heat treated material (with Fe calculated as FeO, see Table 2 and associated table notes), likely due to the loss of H^+ during heating. However, EMP analyses also indicated a stoichiometry that did not significantly change from the

Fe-whitlockite of $Ca_{9.0}Fe_{1.0}(PO_4)_{7.0}$. This EMP result, and the color change, suggested oxidation of Fe^{2+} to Fe^{3+} to produce a ferric Fe-merrillite phase balancing the change in charge due to the loss of H^+ as shown below:

$$Ca_9Fe^{2+}(PO_3OH)(PO_4)_6 \rightarrow Ca_9Fe^{3+}(PO_4)_7. \quad (1)$$

Bond valence calculations (Skowron and Brown, 1990) and Fe – O bond lengths (Table 3) based on SC-XRD analyses of the heat treated material were also consistent with Fe^{3+}. To confirm dehydrogenation, IR analyses were performed on both the unreacted Fe-whitlockite and the heat-treated Fe-merrillite to determine the presence or absence of O–H bonds (Fig. 3A). The IR spectra show a large reduction in absorption between the starting material and the heat-treated material over the range of 3330 to 2570 cm^{-1} where a broad feature is associated with an O–H stretch (White, 1990; Belik et al., 2002). There is also an O–H absorption peak at 2380 cm^{-1} (Belik et al., 2002) which disappears between the starting whitlockite material and the samples heated treated in the Pt crucible open to the atmosphere (Fig. 3A), further supporting the conclusion that the material is ferric (Fe^{3+}) Fe-merrillite. Previous research using solid state methods has also produced a ferric Fe-merrillite (e.g. Lazoryak et al., 1996; Belik et al., 2002), although the material in those experiments was a fine powder.

In order to prevent Fe oxidation and promote the formation of ferrous Fe-merrillite, Fe-whitlockite was heated to 1055 °C in triple argon purged evacuated fused SiO_2 tubes instead of the open air Pt crucible. After heat treatment, EMP analyses indicated a stoichiometry of $Ca_{9.2}Fe_{1.0}Mg_{0.1}(P_{1.0}O_4)_7$ and overall totals rose compared to the starting material (Table 2). Bond valence calculations performed using VALIST (Wills, 1999) and Fe–O bond lengths (Table 3) from SC-XRD data are consistent with an Fe oxidation state of 2+, indicating that the phase is ferrous. However, IR results showed a remaining peak at 2380 cm^{-1} indicating that full

dehydrogenation did not occur during the heat treatment (Fig. 3A). Thus the resulting phase consists of ferrous Fe-merrillite containing some whitlockite. Extending the incubation time at 1055 °C to three days had no effect on the IR results. The result of heat treating the Fe-whitlockite in a sealed SiO_2 appears to be ~80-90% transformation to merrillite based on SC-XRD and is discussed in more detail in the Crystallography section. The incomplete dehydrogenation of the ferrous merrillite may be the result of changing partial pressure due to H^+ loss in the sealed system and warrants further exploration. Many of the heat treated crystals were darker in color suggesting the formation of other, possibly Fe-containing, phases, although BSE and EMP analyses were unable to detect a separate phase within crystals or a color dependent difference in chemistry.

Formation of mixed Fe/Mg-merrillite followed similar trends to that of endmember Fe-merrillite synthesis, with samples heated in open air oxidizing to Fe^{3+}/Mg-merrillite and samples heated in an evacuated SiO_2 tube forming Fe^{2+}/Mg-merrillite. Fe/Mg-whitlockite heat treated in a Pt crucible in open air showed a rise in EMP totals over the starting material beyond that attributable only to total calculations based on Fe_2O_3 rather than FeO (Table 2 and associated table notes). IR analyses, as described above, (Fig. 3B) indicated dehydrogenation had occurred. Bond valence calculations based on SC-XRD data showed that Fe had oxidized to Fe^{3+}, and EMP analyses of the reacted material showed a stoichiometry of $Ca_{9.2}Fe_{0.7}Mg_{0.4}(P_{1.0}O_4)_7$ compared to the unreacted whitlockite of $Ca_{9.0}Fe_{0.7}Mg_{0.3}(P_{1.0}O_3OH)(PO_4)_6$ indicating Ca mobility to balance the change in charge due to the loss of H^+ had occurred. Heat treatment also caused a color change in the material from white/translucent to red/orange.

Dehydrogenation of mixed Fe/Mg-whitlockite by heating in an evacuated fused SiO_2 tube resulted in crystalline material that varied in color from clear translucent to nearly opaque dark

422 black. SC-XRD analysis performed on a clear crystal indicated it to be Fe^{2+}/Mg-merrillite that
423 contained some whitlockite. Fe – O distances determined by SC-XRD indicate that the Fe had
424 not significantly oxidized. A smaller, sharp O-H absorption peak at 2380 cm^{-1} remained (Fig.
425 3B) indicating that the phase contained some whitlockite. Similar to the ferrous endmember Fe-
426 merrillite extending the incubation time to three days had no effect on the IR results. Estimates
427 of the merrillite/whitlockite content are discussed in more detail in the Crystallography section,
428 but indicate that most of the mixed Fe/Mg-reacted material is merrillite (~70%). The color
429 change observed in post heat treatment crystals, as with the Fe-merrillite treated in a SiO_2 tube,
430 suggested the possible formation of another phase. However, as with the similarly treated
431 endmember Fe-whitlockite, BSE and EMP analyses were unable to detect a separate phase
432 within the crystals or a difference in chemistry between lighter or darker colored material.
433 Surface deposits or films on crystals of synthesized endmember and mixed merrillite
434 crystals are apparent under SEM imaging (Figs. 2D to 2F) and by optical microscopy (e.g. Fig.
435 1E). Large (> 150 μm) Mg-merrillite crystals were completely covered with the film, which is
436 generally sub-micron in thickness. The amount of coverage appeared to decrease with
437 decreasing grain size (i.e. smaller crystals exhibited less complete or thinner coverage). In
438 contrast, deposits on Fe^{2+}-bearing crystals rarely covered the entire crystal surface and in the case
439 of ferric Fe-merrillite, most crystals showed no coating (Fig. 1F). SC-XRD analyses did not
440 detect a second phase, although SC-XRD analysis would be unlikely to detect such small
441 amounts of a second phase. The surface textures also lack any morphology that would suggest
442 crystallinity and thus may be amorphous. The coatings were also not detectable in EMP
443 prepared samples due to their sub-micron thickness and similar chemistry. EDS in SEM of the
444 reacted surfaces indicated that the surface deposits were mainly Ca and P with no evidence of

Mg or Fe, and therefore suggest that they may be the result of some form of diffusion to the surface during heating.

In an attempt to determine what additional phases might be present in the merrillite samples, two samples were analyzed by synchrotron XRD; a translucent red-colored crystal of the Fe/Mg-merrillite heat treated in open air (ferric Fe/Mg-merrillite), and a crystal containing a hazy grey to black core within a clear crystal matrix of Fe/Mg-merrillite heat treated in a SiO_2 tube (ferrous Fe/Mg merrillite). Specimens were 100 to 150 μm in diameter. In both cases, diffraction patterns exhibited three distinct sets of features: reflections that belong to multiple domains of merrillite, reflections that belong to domains from whitlockite, and Debye fringes from very fined grained (grainsize < 1μm) inclusions. Thus the samples were not true single crystals.

Modeled and observed patterns of the red-colored ferric Fe/Mg-merrillite sample along with the residual of the fit appear in Figure 4A. In addition to the expected merrillite and whitlockite, monetite and a minor amount of holtedahlite [$Mg_2(PO_4)(OH)$] were also identified. Holtedahlite occurs as a fine grained phase which generated a smooth powder diffraction pattern. With the given experimental settings and based on the observed peak profiles the average grain size of holtdahlite is less than 1 μm and more than 100 nm. Since the diffraction signals from whitlockite, merrillite, and monetite were not powderous, a Reitveld analysis for phase quantification could not be conducted. However, the strength of the diffraction signal of holtedahlite indicates that it is significantly less than merrillite, whitlockite, and monetite.

The ferrous Fe/Mg-merrillite specimen with the grey-black core region was composed of a solid solution whitlockite/merrillite matrix (>3 micron grain size) containing small amounts of monetite and an additional unidentified fine grained (< 1μm) phase. Limited diffraction data are

consistent with a Na-bearing Ca-ferrate, although a confident identification is not possible and oxidized Fe would be surprising in the ferrous Fe/Mg-merrillite. The observed pattern with the whitlockite/merrillite contributions masked and modeled patterns of monetite, a Na-bearing Ca-Ferrate, and the residual of the fit appear in Figure 4B.

Presumably, some of these additional phases may also occur in the endmember merrillite materials, though we were not able to confirm that as part of the current study. Synchrotron diffraction patterns of monetite might explain the calcium and phosphorus phase observed as films on crystals. SC-XRD analyses did not detect monetite, holtedahlite or another unidentified phase, but the technique and sample selection criteria are designed to refine single structures from single crystals and are not applicable to detecting minor phases that exhibit reflections from multiple domains or powder fringe patterns.

The mechanism by which calcium balances the charge imbalance due to the loss of H^+ from whitlockite and increases the stoichiometric Ca in non-ferric merrillite is unclear. Gopal and Calvo (1972) and Gopal et al. (1974), who synthesized merrillite from both natural and synthetic Mg-whitlockite, present no mechanism. Hughes et al. (2008), who synthesized merrillite from synthetic Mg-whitlockite, suggest Ca-rich reagents entrained in the synthetic whitlockite crystals yielded Ca sufficient to counter the charge imbalance due to H^+ loss, with the Ca presumably diffusing through the crystal. However, this mechanism fails to explain enhanced Ca concentrations in the whitlockite to merrillite dehydrogenation experiments of Gopal and Calvo (1972) who used natural whitlockite, which would contain no entrained reagents.

The apparent enrichment of Ca relative to phosphate during the whitlockite to merrillite transformation could take place through the formation of additional phases that either diffuse to

the surface or are dispersed and difficult to detect within the bulk crystals. This would be consistent with the synchrotron diffraction data that indicate additional phases were present within Fe/Mg-merrillites. An additional phase or phases, like the holtedahlite or Fe-bearing phase indicated by synchrotron diffraction, would be required in order to take up extra Mg or Fe made available during the transformation from whitlockite to merrillite. Synchrotron diffraction data from the ferric Fe/Mg-merrillite heat treated open to atmosphere indicated holtedahlite as the only additional crystalline phase beyond monetite, which would take up remaining Mg. It is plausible that if the Fe is oxidizing during transformation as per Equation 1, an additional Fe-bearing phase may not necessarily form. However, in the case of the ferrous Fe/Mg-merrillite treated in the SiO_2 sealed tube, both Fe- and Mg-bearing additional phases would be expected and synchrotron diffraction data only indicate a possible Fe-bearing crystalline phase. It is possible that an undetected amorphous Mg-phase is taking up the excess Mg, and that a similar Fe-bearing phase may also form to take up any excess Fe in the Ferric merrillite that is not accounted for by oxidation (Equation 1). Candidates for such a phase include Fe- and Mg-pyrophosphates [$X_2(P_2O_7)$ where X is Mg or Fe], which can be produced in high temperature metal/phosphate systems and can be amorphous (Bensalem et al., 1997; Lee et al., 2012). These Fe- and Mg-pyrophosphate phases may also act as transitional phases – for example, a hypothetical Mg-pyrophosphate may be a transitional phase to the holtedahlite observed by synchrotron XRD (Equation. 2), which would explain why holtedahlite was detected in one sample, but no Mg-containing phase in the other:

$$Mg_2(P_2O_7) + 2\ H_2O \rightarrow\ Mg_2(PO_4)(OH) + H_3PO_4 \qquad (2).$$

A general reaction reflecting the transformation from whitlockite to merrrillite may therefore include either holtedahlite or an amorphous metal pyrophosphate, and be represented by:

$$\textit{Whitlockite} + \textit{Heat} \rightarrow \textit{Merrillite} + \textit{Monetite} + \textit{Additional Phase(s)} + H_3PO_4 + H_2O,$$

where non-merrillite phases take up any remaining chemistry resulting from the whitlockite-to-merrillite transformation. A balanced example that includes both monetite and pyrophosphate as the metal phosphate is:

$$24\ Ca_9X(PO_3OH)(PO_4)_6 \rightarrow\ 22\ Ca_{9.5}X(PO_4)_7\ +7\ Ca(HPO_4) + X_2(P_2O_7) + 5\ H_3PO_4 + H_2O \quad (3).$$

Equations similar to 1, 2, or 3, or combinations thereof, are consistent with the observations of this study and allow for a mechanism of charge balance that does not require entrained synthesis reagents. Such a mechanism would better explain the transformation of natural whitlockite to merrillite confirmed by Gopal and Calvo (1972), where no entrained reagents from synthesis were present.

Crystallography

The atomic parameters of Mg-whitlockite and Mg-merrillite synthesized by conceptually similar methods to those used here have been previously measured by SC-XRD and discussed (Gopal et al., 1974; Hughes et al., 2008), and therefore we only focus on differences between the Fe- and Fe/Mg-whitlockite and merrillite structures determined in this work. The structures of Fe-whitlockite and ferric Fe-merrillite have been previously refined using powder XRD diffraction (Corlett and Keppler, 1966; Keppler, 1968; Lazoryak et al., 1996; Belik et al., 2002). Belik et al. (2002) utilized neutron powder XRD and located two deuterium sites for Fe–whitlockite; hydrogen cannot be located by SC-XRD methods. Since significantly more accuracy is possible with single crystal XRD, we report the structures of Fe-whitlockite and ferric Fe-merrillite here (Table 4). Atomic parameters of synthetic ferrous Fe-merrillite, and mixed Fe/Mg-merrillite do not appear to be in the literature, and we present atomic coordinates and full listing of bond distances as Tables A2 and A3 in deposit materials[1]. A .cif file containing all six crystal structures has also been deposited[1].

Broadly speaking, the six crystal structures determined (Fe- and Fe/Mg-whitlockite, as well as ferrous and ferric Fe- and Fe/Mg-merrillite)(Table 4) are similar with differences related mainly to the chemistry. The position of the proton has previously been established as protonating the phosphate group located on the 3-fold axis (labeled P3 in this work). Protonated phosphates point in the opposite direction compared to non-protonated phosphates. Modeling of this disorder for the synthetic Fe-whitlockite found 89.0% of P3 on the inverted site; 100% should be inverted if the structure were fully protonated. It is possible that some protons occupy other sites in the structure, some Fe^{3+} is present, minor merrillite is present, or a combination of the three. Small amounts of merrillite within natural whitlockite and synthetic Mg-whitlockite have been previously noted (Hughes et al., 2008).

Heat treating the Fe-whitlockite in a Pt crucible open to the atmosphere yields an Fe-merrillite sample where 97.1% of the P3 are not on the inverted site, in agreement with essentially full conversion to merrillite. This does not require 2.9% protonation – it is possible that a fraction of the P3 phosphate remains inverted after deprotonation. The observed Fe – O distances (Table 3) are highly sensitive to the oxidation state of the iron. We find distances in the Fe-whitlockite sample (Fe-O bond lengths of ~2.03 Å), and in the ferric merrillite sample (Fe-O bond length of ~2.10 Å) that match expected metal – oxygen distances for Fe^{2+} and Fe^{3+}, respectively. Note that the approximate difference of 0.1 Å between Fe for Fe^{2+} and Fe^{3+} is larger by roughly a factor of 50 than standard deviations on these bond distances (Table 3). Bond valence calculations are normally only an approximate method of identifying oxidation state as bond distances can be influenced by a variety of structural features in a specific compound. In this particular instance, bond valence calculations are more conclusive as the crystal structures and compositions are very similar to each other. While the observed bond

distances as well as the bond valence calculations clearly suggest primarily Fe^{2+} in the Fe-whitlockite and ferrous merrillite, and primarily Fe^{3+} in ferric merrillite, they only indicate which oxidation state is predominant in each structure, not the relative amounts of Fe^{2+} and Fe^{3+}.

Heating the Fe-whitlockite samples in evacuated SiO_2 tubes apparently prevented some oxidation of Fe^{2+} to Fe^{3+}, as evidenced by little change in the measured Fe – O bond distances (Table 3). Charge balance in the merrillite is maintained by the migration of Ca^{2+} cation sites to around where protons are found in the whitlockite form. The Ca is distributed over two sites, Ca4A and Ca4B, with refined occupancies of 14.8 and 29.6%, respectively. As it is not possible from crystallography to assign elements to partially occupied sites such as these, we infer that they are likely Ca based on its increase in microprobe data (Table 2) and the bonding environments for both sites. Table 3 includes bond distances for these sites, all of which are longer than expected for Fe^{2+}. In addition, the environments are quite irregular, which would be unfavorable for d^6 Fe but not unusual for Ca^{2+}. As 50% occupancy of a divalent cation site would provide sufficient charge balance to replace that lost by full dehydrogenation, these occupancies are consistent with 88.8% conversion to merrillite. Of the P3 phosphates, 23.9% are inverted, which is consistent with a modestly higher degree of protonation than suggested by the Ca^{2+} occupancies, though some of the P3 phosphate may have remained inverted after deprotonation. The Ca^{2+} occupancies of the Fe-whitlockite heat treated in a sealed SiO2 tube, together with P3 observations, indicate ~80-90% conversion to merrillite. There was no evidence of significant electron density on or around these sites in the Fe-whitlockite and Fe-merrillite heat treated in a Pt crucible.

The mixed Fe/Mg-whitlockite sample refined to a similar overall structure as the pure Fe-whitlockite. Refinement of the Fe/Mg ratio yielded a 63.7% Fe occupancy, with the balance Mg,

in general agreement with the microprobe results (Table 2). The Fe/Mg ratios refined for the two heated samples refined to 75.4% (Pt crucible) and 64.6% (SiO_2 tube). Inter-crystal standard deviations on this ratio determined by microprobe were high, so it is quite possible that this value varies some from crystal to crystal. P3 phosphates are inverted 84.0% of the time, suggesting the whitlockite is 16% merrillite already, and the Fe – O distances are consistent with Fe^{2+}. The sample heated in air ended up with 6.5% of the P3 site inverted, suggesting near complete conversion to merrillite structure, and the Fe – O distances are consistent with Fe^{3+}.

Results of heating mixed Fe/Mg samples in sealed SiO_2 tubes were also quite similar to the pure Fe case. Fe – O distances are consistent with Fe^{2+}, and 30.9% of the P3 phosphate group are inverted, indicating that the sample is largely merrillite. Two Ca sites with similar environments and occupancies (9.8% and 26.4%) were also found.

Implications for Martian Studies

Merrillite is a potentially important indicator of martian geologic processes, including the evolution of halogen and water content over time in martian magmas. A deeper understanding of the relationship of merrillite formation to halogen and water content in melts may hold clues to parts of the martian igneous and hydrologic cycles. The relationship of merrillite/whitlockite to apatite in melts may also hold important clues to the evolution of not only martian magmas, but those of other differentiated bodies including Earth and asteroids. The phosphate in martian soils and dust may also be present as merrillite, making the mineral of interest to martian surface process studies and, as a major source of bio-essential phosphate, studies pertaining to martian habitability. Access to a supply of synthetic, coarse crystalline whitlockite and merrillite of

various chemistries and an understanding of the conditions under which these phases can be formed, as presented here, will likely aid in facilitating a number of these studies as well as further investigations into more fundamental thermodynamic and kinetic parameters of the minerals. Complete dehydrogenation of ferrous merrillite in this study may have been hindered by the sealed tube used. A flow through apparatus may eventually prove more successful, and while Na^+ incorporation into merrillite may not be possible under hydrothermal conditions, a high temperature approach may yield success. Future efforts in producing completely dehydrogenated ferrous merrillite as well as incorporating Na^+ into synthetic merrillite are warranted as the conditions under which these are achieved may reveal further insights into the natural environments, martian or otherwise, in which these minerals form.

Acknowledgements

This material is based upon work supported by the National Aeronautics and Space Administration (NASA) Mars Fundamental Research Program grant NNX10AP58G to E. M. Hausrath, a Nevada Space Grant Consortium fellowship to C. T. Adcock, a GSA research grant to C. T. Adcock, and by a cooperative agreement through the National Nuclear Security Administration under the Stewardship Science Academic Alliances program through DOE Cooperative Agreement #DE-NA0001982 to P. M. Forster and O. Tsauner. The authors thank David Hatchett and Keith Lawler for IR spectroscopy support, as well as Ravhi Kumar, Darius Roohani, and Michael Steiner for aid in synthesis experiments. The comments and advice of Francis McCubbin and Justin Filiberto who reviewed the manuscript were greatly appreciated and improved many aspects of the final manuscript. We also express our appreciation to Eugene Smith, Henry Sun, Sean Mulcahy, Valerie Tu, William Kerlin, and Seth Gainey for technical

632 assistance and discussion which improved this paper. The Advanced Light Source is supported
633 by the Director, Office of Science, Office of Basic Energy Sciences, of the U.S. Department of
634 Energy under Contract No. DE-AC02-05CH11231.

635

636

637 ## References

638 Adcock, C., Hausrath, E., and Forster, P. (2013) Readily available phosphate from minerals in early
639 aqueous environments on Mars. Nature Geoscience, 6(10), 824-827.
640 Belik, A., Izumi, F., Stefanovich, S.Y., Lazoryak, B., and Oikawa, K. (2002) Chemical and Structural
641 Properties of a Whitlockite-like Phosphate, Ca9FeD(PO4)7. Chemistry of Materials, 14(9), 3937-
642 3945.
643 Bensalem, A., Ahluwalia, M., Vijayaraghavan, T.V., and Ko, Y.H. (1997) Synthesis of amorphous
644 MgHPO4 · x(R) [R = Ethanol; Ethylene glycol] in anhydrous media. Materials Research Bulletin,
645 32(11), 1473-1483.
646 Bergerhoff, G., and Brown, I. (1987) Crystallographic databases. International Union of Crystallography,
647 Chester, 77-95.
648 Brückner, J., Dreibus, G., Gellert, R., Squyres, S.W., Wänke, H., Yen, A., and Zipfel, J. (2008) Mars
649 Exploration Rovers: chemical composition by the APXS. In J. Bell, Ed. The Martian Surface -
650 Composition, Mineralogy, and Physical Properties, p. 58-100. Cambridge University Press,
651 Cambridge.
652 Corlett, M., and Keppler, U. (1966) Chemische Zusammensetzung des Whitlockits. Naturwissenschaften,
653 53(4), 105-105.
654 Dolomanov, O.V., Bourhis, L.J., Gildea, R.J., Howard, J.A., and Puschmann, H. (2009) OLEX2: a
655 complete structure solution, refinement and analysis program. Journal of Applied
656 Crystallography, 42(2), 339-341.
657 Dorozhkin, S.V., and Epple, M. (2002) Biological and medical significance of calcium phosphates.
658 Angewandte Chemie International Edition, 41(17), 3130-3146.
659 Downs, R.T., and Hall-Wallace, M. (2003) The American Mineralogist crystal structure database.
660 American Mineralogist, 88(1), 247-250.

661 Dowty, E. (1977) Phosphate in Angra dos Reis: Structure and composition of the Ca3(PO4)2 minerals.
662 Earth and Planetary Science Letters, 35(2), 347-351.
663 Filiberto, J., and Treiman, A.H. (2009) The effect of chlorine on the liquidus of basalt: First results and
664 implications for basalt genesis on Mars and Earth. Chemical Geology, 263(1-4), 60-68.
665 Frondel, C. (1941) Whitlockite: a new calcium phosphate Ca3 (PO4) 2. American Mineralogist, 26, 145-
666 152.
667 Frondel, C., and Prien, E.L. (1946) Deposition of Calcium Phosphates Accompanying Senile
668 Degeneration and Disease. Science, 103(2672), 326.
669 Fuchs, L.H. (1962) Occurrence of Whitlockite in Chondritic Meteorites. Science, 137(3528), 425-426.
670 Goetz, W., Bertelsen, P., Binau, C.S., Gunnlaugsson, H.P., Hviid, S.F., Kinch, K.M., Madsen, D.E.,
671 Madsen, M.B., Olsen, M., and Gellert, R. (2005) Indication of drier periods on Mars from the
672 chemistry and mineralogy of atmospheric dust. Nature, 436(7047), 62-65.
673 Gopal, R., and Calvo, C. (1972) Structural Relationship of Whitlockite and βCa3(PO4)2. Nature, 237(71),
674 30-32.
675 Gopal, R., Calvo, C., Ito, J., and Sabine, W.K. (1974) Crystal-Structure of Synthetic Mg-Whitlockite,
676 Ca18Mg2H2(PO4)14. Canadian Journal of Chemistry-Revue Canadienne De Chimie, 52(7),
677 1155-1164.
678 Greenwood, J.P., and Blake, R.E. (2006) Evidence for an acidic ocean on Mars from phosphorus
679 geochemistry of Martian soils and rocks. Geology, 34(11), 953-956.
680 Gross, J., Filiberto, J., and Bell, A.S. (2013a) Water in the martian interior: Evidence for terrestrial
681 MORB mantle-like volatile contents from hydroxyl-rich apatite in olivine–phyric shergottite
682 NWA 6234. Earth and Planetary Science Letters.
683 Gross, J., Filiberto, J., Herd, C.D., Daswani, M.M., Schwenzer, S.P., and Treiman, A.H. (2013b)
684 Petrography, mineral chemistry, and crystallization history of olivine-phyric shergottite NWA
685 6234: A new melt composition. Meteoritics & Planetary Science.
686 Gulick, A. (1955) Phosphorus as a Factor in the Origin of Life. American Scientist, 43(3), 479-489.

687 Hamad, M., and Heughebaert, J.-C. (1986) The growth of whitlockite. Journal of Crystal Growth, 79(1),
688 192-197.
689 Hammersley, A., Svensson, S., Hanfland, M., Fitch, A., and Hausermann, D. (1996) Two-dimensional
690 detector software: from real detector to idealised image or two-theta scan. International Journal of
691 High Pressure Research, 14(4-6), 235-248.
692 Hausrath, E., Golden, D., Morris, R., Agresti, D., and Ming, D. (2013) Acid sulfate alteration of
693 fluorapatite, basaltic glass and olivine by hydrothermal vapors and fluids: Implications for
694 fumarolic activity and secondary phosphate phases in sulfate-rich Paso Robles soil at Gusev
695 Crater, Mars. Journal of Geophysical Research: Planets.
696 Hausrath, E.M., and Tschauner, O. (2013) Natural Fumarolic Alteration of Fluorapatite, Olivine, and
697 Basaltic Glass, and Implications for Habitable Environments on Mars. Astrobiology, 13(11),
698 1049-1064.
699 Hughes, J.M., Jolliff, B.L., and Gunter, M.E. (2006) The atomic arrangement of merrillite from the Fra
700 Mauro Formation, Apollo 14 lunar mission: The first structure of merrillite from the Moon.
701 American Mineralogist, 91(10), 1547-1552.
702 Hughes, J.M., Jolliff, B.L., and Rakovan, J. (2008) The crystal chemistry of whitlockite and merrillite and
703 the dehydrogenation of whitlockite to merrillite. American Mineralogist, 93(8-9), 1300-1305.
704 Jarcho, M., Salsbury, R., Thomas, M., and Doremus, R. (1979) Synthesis and fabrication of β-tricalcium
705 phosphate (whitlockite) ceramics for potential prosthetic applications. Journal of Materials
706 Science, 14(1), 142-150.
707 Jarosewich, E. (2002) Smithsonian microbeam standards. JOURNAL OF RESEARCH-NATIONAL
708 INSTITUTE OF STANDARDS AND TECHNOLOGY, 107(6), 681-686.
709 Jolliff, B.L., Haskin, L.A., Colson, R.O., and Wadhwa, M. (1993) Partitioning in REE-saturating
710 minerals: Theory, experiment, and modelling of whitlockite, apatite, and evolution of lunar
711 residual magmas. Geochimica et Cosmochimica Acta, 57(16), 4069-4094.

712 Jolliff, B.L., Hughes, J.M., Freeman, J.J., and Zeigler, R.A. (2006) Crystal chemistry of lunar merrillite
713 and comparison to other meteoritic and planetary suites of whitlockite and merrillite. American
714 Mineralogist, 91(10), 1583-1595.
715 Keppler, U. (1968) Structural investigation of calciumphosphate and isotypic structures. Bulletin de la
716 Société Chimique de France.
717 Lagier, R., and Baud, C.-A. (2003) Magnesium whitlockite, a calcium phosphate crystal of special
718 interest in pathology. Pathology-Research and Practice, 199(5), 329-335.
719 Lane, M.D., Bishop, J.L., Darby Dyar, M., King, P.L., Parente, M., and Hyde, B.C. (2008) Mineralogy of
720 the Paso Robles soils on Mars. American Mineralogist, 93(5-6), 728-739.
721 Lazoryak, B., Morozov, V., Belik, A., Khasanov, S., and Shekhtman, V.S. (1996) Crystal Structures and
722 Characterization of Ca 9 Fe (PO 4) 7 and Ca 9 FeH 0.9 (PO 4) 7. Journal of Solid State
723 Chemistry, 122(1), 15-21.
724 Le Bail, A. (2005) Whole powder pattern decomposition methods and applications: a retrospection.
725 Powder Diffraction, 20(4), 316-326.
726 Lee, G.-H., Seo, S.-D., Shim, H.-W., Park, K.-S., and Kim, D.-W. (2012) Synthesis and Li electroactivity
727 of Fe2P2O7 microspheres composed of self-assembled nanorods. Ceramics International, 38(8),
728 6927-6930.
729 McCubbin, F.M., and Nekvasil, H. (2008) Maskelynite-hosted apatite in the Chassigny meteorite:
730 Insights into late-stage magmatic volatile evolution in martian magmas. American Mineralogist,
731 93(4), 676-684.
732 McGuire, A.V., Francis, C.A., and Dyar, M.D. (1992) Mineral standards for electron microprobe analysis
733 of oxygen. American Mineralogist, 77, 1087-1087.
734 McSween, H., and Treiman, A.H. (1998) Martian Meteorites. In J. Papike, Ed. Planetary Materials, p. F1-
735 F53. Mineral Society of America, Washington, DC.

McSween, H.Y., Eisenhour, D.D., Taylor, L.A., Wadhwa, M., and Crozaz, G. (1996) QUE94201 shergottite: Crystallization of a Martian basaltic magma. Geochimica et Cosmochimica Acta, 60(22), 4563-4569.

Merrill, G.P. (1915) On the Monticellite-Like Mineral in Meteorites, and on Oldhamite as a Meteoric Constituent. Proceedings of the National Academy of Sciences, 1(5), 302-308.

-. (1917) On the calcium phosphate in meteoric stones. American Journal of Science(256), 322-324.

Orlova, A.I., Khaĭnakov, S., Loginova, E., Oleneva, T., Granda, S.G., and Kurazhkovskaya, V.S. (2009) Calcium thorium phosphate (Whitlockite-type mineral). Synthesis and structure refinement. Crystallography Reports, 54(4), 591-597.

Patiño Douce, A.E., and Roden, M. (2006) Apatite as a probe of halogen and water fugacities in the terrestrial planets. Geochimica et Cosmochimica Acta, 70(12), 3173-3196.

Patiño Douce, A.E., Roden, M.F., Chaumba, J., Fleisher, C., and Yogodzinski, G. (2011) Compositional variability of terrestrial mantle apatites, thermodynamic modeling of apatite volatile contents, and the halogen and water budgets of planetary mantles. Chemical Geology, 288(1), 14-31.

Rowles, S. (1968) The precipitation of whitlockite from aqueous solutions. Bull Soc Chim Fr, 1968, 802.

Rubin, A.E. (1997) Mineralogy of meteorite groups: An update. Meteoritics & Planetary Science, 32(5), 733-734.

Ruszala, F., and Kostiner, E. (1980) The hydrothermal synthesis and crystal growth of various whitlockites and a manganese containing graftonite. Journal of Crystal Growth, 48(3), 473-474.

Schwartz, A.W. (2006) Phosphorus in Prebiotic Chemistry. Philosophical Transactions: Biological Sciences, 361(1474), 1743-1749.

Shearer, C., Papike, J., Burger, P., Sutton, S., McCubbin, F., and Newville, M. (2011a) Direct determination of europium valence state by XANES in extraterrestrial merrillite: Implications for REE crystal chemistry and martian magmatism. American Mineralogist, 96(8-9), 1418-1421.

760 Shearer, C.K., Burger, P.V., Papike, J.J., Sharp, Z.D., and McKeegan, K.D. (2011b) Fluids on
761 differentiated asteroids: Evidence from phosphates in differentiated meteorites GRA 06128 and
762 GRA 06129. Meteoritics & Planetary Science, 46(9), 1345-1362.
763 Sheldrick, G.M. (2007) A short history of SHELX. Acta Crystallographica Section A: Foundations of
764 Crystallography, 64(1), 112-122.
765 Skowron, A., and Brown, I. (1990) Refinement of the structure of robinsonite, Pb4Sb6S13. Acta
766 Crystallographica Section C: Crystal Structure Communications, 46(4), 527-531.
767 Terada, K., Monde, T., and Sano, Y. (2003) Ion microprobe U-Th-Pb dating of phosphates in martian
768 meteorite ALH 84001. Meteoritics & Planetary Science, 38(11), 1697-1703.
769 Teterskii, A., Stefanovich, S.Y., Lazoryak, B., and Rusakov, D. (2007) Whitlockite solid solutions Ca9−
770 x M x R (PO4) 7 (x= 1, 1.5; M= Mg, Zn, Cd; R= Ln, Y) with antiferroelectric properties. Russian
771 Journal of Inorganic Chemistry, 52(3), 308-314.
772 Treiman, A.H. (2003) Chemical compositions of martian basalts (shergottites): Some inferences on b;
773 formation, mantle metasomatism, and differentiation in Mars. Meteoritics & Planetary Science,
774 38(12), 1849-1864.
775 Westheimer, F.H. (1987) Why Nature Chose Phosphates. Science, 235(4793), 1173-1178.
776 Wherry, E. (1917) Merrillite, meteoritic calcium phosphate. American Mineralogist, 2, 119.
777 White, R. (1990) Chromatography/Fourier transform infrared spectroscopy and its applications. CRC
778 Press.
779 Wills, A.S. (1999) VaList-bond valence calculation and listing Program, www.ccp14.ac.uk
780 Xie, X., Minitti, M.E., Chen, M., Mao, H.-k., Wang, D., Shu, J., and Fei, Y. (2002) Natural high-pressure
781 polymorph of merrillite in the shock veins of the Suizhou meteorite. Geochimica et
782 Cosmochimica Acta, 66(13), 2439-2444.
783

Figure Captions

Figure 1. Optical images of synthesized phases. **A)** Mg-whitlockite single crystals with a polycrystalline aggregate in the upper left corner. **B)** Fe-whitlockite single crystal. Dark color inside crystal suggests some intra-crystalline iron film on growth faces. **C)** Fe-whitlockite polycrystalline aggregates. Darker colors in some aggregates from inter-crystalline iron films. **D)** Mixed Fe/Mg-whitlockite single crystals. **E)** Mg-merrillite showing the hazy surface texture due to a thin film deposit post heat treatment. The extent of coverage appeared to decrease with decreasing grain size (i.e. smaller crystals exhibited less complete or thinner coverage). **F)** Ferric Fe-merrillite crystals showing the incomplete hazy surface texture post heat treatment on some crystals (arrows). Deposits on the minerals rarely covered the entire crystalline surface. "White crystals" in this image are polycrystalline aggregates.

Figure 2. Scanning Electron Microscope images of synthesized materials. **A)** SEM SEI image of synthesized Mg-whitlockite. **B)** SEM SEI image of synthetic twinned Fe-whitlockite. **C)** SEM SEI image of synthesized Fe/Mg-whitlockite. **D)** SEM SEI with inset (taken at 3000x) showing coating developed on Mg-merrillite crystal during synthesis. Most Mg-merrillite crystals were completely covered, although smaller grains exhibited less complete or thinner coverage. **E)** SEM SEI image of Ferric Fe-merrillite showing coating developed during synthesis. In contrast to Mg-merrillite, the deposit on the mineral rarely covered the entire crystalline surface and in some cases crystal showed no coating, consistent with discussion of our proposed mechanisms. **F)** SEM SEI image of ferrous Fe-merrillite showing coating developed during synthesis.

Figure 3. IR Spectra of **A)** Fe-whitlockite, ferrous merrillite treated in a SiO_2 tube, and ferric merrillite treated open to atmosphere. **B)** Fe/Mg-whitlockite, ferrous Fe/Mg-merrillite heat treated in a SiO_2 tube, and ferric Fe/Mg-merrillite heat treated open to atmosphere. Whitlockite data show an apparent absorption from 3330 to 2570 cm^{-1} where a broad O-H stretch feature exists. The absorbance is mainly absent in material treated in a Pt crucible exposed to air (ferric Fe- and Fe/Mg-merrillite), with some absorption in the O-H stretching band present in material treated in a sealed SiO_2 tube (ferrous Fe- and Fe/Mg-merrillite) including a peak at 2380 cm^{-1}. Spectra offset for clarity.

Figure 4. Synchrotron X-ray diffraction. **A)** Observed and modeled patterns of the red-colored ferric Fe/Mg-merrillite sample along with the residual of the fit. Beyond the expected whitlockite/merrillite observed in the crystal, monetite and holtedahlite also appear to be present. **B)** Similar data for a dark-colored ferrous merrillite crystal with whitlockite/merrillite pattern data masked out. This crystal also contained monetite and an additional unconfirmed phase with structure similar to a ferrate.

817

818 # Tables

819

Table 1. Masses and volumes used in finalized whitlockite synthesis methods

Synthetic Mineral	*$MgNO_3$ (g)*	*FeS (g)*	*NaCl (g)[a]*	*HAP (g)[b]*	*Total solid Mass (g)*	*H_2O (ml)*	*Solids in Solution (g/L)*
Mg-whitlockite	0.300 (±0.003)	-	-	1.000 (±0.003)	1.300	90	14.4
Fe-whitlockite	-	0.055 (±0.005)		1.000 (±0.003)	1.055	90	11.7
Fe/Mg-whitlockite	0.050 (±0.003)	0.050 (±0.005)	0.067 (±0.005)	1.000 (±0.003)	1.167	90	13.0

820 *[a]Later experiments showed NaCl to have no effect on synthesis. [b]HAP = hydroxyapatite.*

821

822

Table 2. Chemical analyses of whitlockite and merrillite by electron microprobe in wt%.

	Mg-whitlockite		*Mg-merrillite*	
CaO	47.61	(0.20)	48.89	(0.21)
P_2O_5	46.85	(0.27)	46.38	(0.32)
MgO	3.54	(0.14)	4.06	(0.12)
FeO	0.02	(0.03)	0.02	(0.03)
Na_2O	B.D.		B.D.	
[a]H_2O	0.86		-	
Total	98.02	(0.34)	99.35	(0.36)
N	17		16	
Stoic.	$Ca_{9.0}Mg_{0.9}(PO_3OH)(PO_4)_6$		$Ca_{9.4}Mg_{1.1}(PO_4)_{7.0}$	

	Fe-whitlockite		*Ferric Fe-merrillite (Pt cruc.)*		*Ferrous Fe-merrillite (SiO_2 tube)*	
CaO	46.00	(0.45)	46.37	(0.27)	47.00	(0.19)
P_2O_5	45.26	(0.47)	46.02	(0.50)	45.42	(0.46)
MgO	0.14	(0.03)	0.34	(0.07)	0.39	(0.10)
[b]Fe_2O_3	-		6.74	-	-	
FeO	6.75	(0.27)	-		6.85	(0.18)
Na_2O	B.D		B.D.		B.D.	
[a]H_2O	0.86		-		-	
Total	98.15	(0.63)	99.47	(0.45)	99.65	(0.53)
N	18		17		20	
Stoic.	$Ca_{9.0}Mg_{0.9}(PO_3OH)(PO_4)_6$		$Ca_{9.0}Fe_{0.9}Mg_{0.1}(PO_4)_{7.0}$		$Ca_{9.2}Fe_{1.0}Mg_{0.1}(PO_4)_{7.0}$	

	Fe/Mg-whitlockite		*Ferric Fe/Mg-merrillite (Pt cruc.)*		*Ferrous Fe/Mg-merrillite (SiO_2 tube)*	
CaO	46.54	(0.59)	46.79	(0.33)	47.09	(0.22)
P_2O_5	45.83	(0.36)	45.96	(0.39)	45.40	(0.38)
MgO	1.00	(0.20)	1.29	(0.09)	1.20	(0.16)
[b]Fe_2O_3	-		4.98	-	-	
FeO	4.62	(0.71)	-		5.68	(0.23)
Na_2O	B.D.		B.D.		B.D.	
[a]H_2O	0.86		-		-	
Total	97.99	(0.49)	99.02	(0.60)	99.36	(0.48)
n	15		13		19	
Stoic.	$Ca_{9.0}Fe_{0.7}Mg_{0.3}(PO_3OH)(PO_4)_6$		$Ca_{9.1}Fe_{0.7}Mg_{0.3}(PO_4)_{7.0}$		$Ca_{9.2}Fe_{0.9}Mg_{0.3}(PO_4)_{7.0}$	

Parenthetical values are 1 standard deviation. n = number of analyses averaged chemistry is based on. B.D. = below detection.

[a]H_2O is based on ideal whitlockite (Hughes et al., 2008) and is not included in the EMP totals.

[b]Fe was measured assuming Fe^{2+} and recalculated to Fe^{3+} with total and resulting stoichiometry adjusted accordingly. For ferric Fe-merrillite, the original FeO wt. % = 6.07 with a standard deviation of 0.13, analysis total of 98.80,and calculated stoichiometry of $Ca_{9.1}Fe_{0.9}Mg_{0.1}(PO_4)_{7.0}$. For Ferric Fe/Mg-merrillite the original FeO wt. % = 4.48 with a standard deviation of 0.08, analysis total of 98.53,and calculated stoichiometry of $Ca_{9.2}Fe_{0.7}Mg_{0.4}(PO_4)_{7.0}$. NOTE: It is not possible by microprobe alone to actually determine Fe^{2+}/Fe^{3+} content and these values are estimates.

835
836

Table 3. Select bond lengths discussed in text for synthetic minerals Å.

		Fe-whitlockite	Fe/Mg-whitlockite	Ferric Fe-merrillite (Pt cruc.)	Ferrous Fe-merrillite (SiO_2 tube)	Ferric Fe/Mg-merrillite (Pt cruc.)	Ferrous Fe/Mg-merrillite (SiO_2 tube)
Fe(1)-	O(4)	2.1131(16)	2.1067(13)	2.046(2)	2.122(3)	2.048(2)	2.104(2)
	O(4)#1	2.1130(16)	2.1068(13)	2.046(2)	2.122(3)	2.048(2)	2.104(2)
	O(4)#2	2.1130(16)	2.1068(13)	2.046(2)	2.122(3)	2.048(2)	2.104(2)
	O(5)	2.0893(16)	2.0806(12)	2.011(2)	2.108(3)	2.023(2)	2.092(2)
	O(5)#1	2.0893(16)	2.0806(12)	2.011(2)	2.108(3)	2.023(2)	2.092(2)
	O(5)#2	2.0893(16)	2.0806(12)	2.011(2)	2.108(3)	2.023(2)	2.092(2)
Ca(4A)-	O(6)#18	NA	NA	NA	2.736(5)	NA	2.758(6)
	O(6)#19	NA	NA	NA	2.736(5)	NA	2.758(6)
	O(7)#18	NA	NA	NA	2.541(4)	NA	2.541(4)
	O(7)#19	NA	NA	NA	2.541(4)	NA	2.541(4)
Ca(4B)-	O(6)#18	NA	NA	NA	2.516(3)	NA	2.518(2)
	O(6)#19	NA	NA	NA	2.516(3)	NA	2.518(2)
	O(7)#18	NA	NA	NA	2.846(5)	NA	2.851(4)
	O(7)#19	NA	NA	NA	2.846(5)	NA	2.851(4)

837 *Parenthetical values are standard deviations. "Pt cruc." denotes merrillite produced in a platinum crucible in open*
838 *air. "SiO_2 Tube" denotes merrillite produced using a triple argon purged and seal glass tube. Only Fe-O and Ca-O*
839 *bonds discussed in text appear in table. A full table of bond lengths appears in deposit item Table A4.*

Table 4. Single crystal X-ray diffraction refinement statistics

Mineral	Fe-whitlockite	Fe/Mg-whitlockite	Ferric Fe-merrillite (Pt cruc.)	Ferrous Fe-merrillite (SiO_2 tube)	Ferric Fe/Mg-merrillite (Pt cruc.)	Ferrous Fe/Mg-merrillite (SiO_2 tube)
Emp. formula	$Ca_9FeHO_{28}P_7$	$Ca_9Fe_{0.64}HMg_{0.36}O_{28}P_7$	$Ca_9FeH_{0.02}O_{28}P_7$	$Ca_{9.44}FeH_{0.12}O_{28}P_7$	$Ca_9Fe_{0.75}Mg_{0.25}O_{28}P_7$	$Ca_{9.36}Fe_{0.65}H_{0.28}Mg_{0.35}O_{28}P_7$
Formula wt.	1082.37	1070.93	1081.38	1099.12	1073.59	1084.98
a (Å)	10.3510(7)	10.3499(4)	10.3278(11)	10.3453(6)	10.3301(13)	10.3392(7)
c (Å)	37.059(2)	37.0715(16)	37.050(4)	37.118(2)	37.062(5)	37.081(2)
Volume ($Å^3$)	3438.6(4)	3439.1(2)	3422.4(8)	3440.3(5)	3425.1(10)	3432.8(5)
Density (calc.) (Mg/m^3)	3.136	3.103	3.148	3.183	3.123	3.149
Reflections collected	17516	17609	17589	11475	17501	17513
Independent reflections	2352	2355	2334	2238	2338	2342
R(int)	0.0221	0.0202	0.0248	0.0236	0.0249	0.0213
parameters	140	142	140	146	143	153
Goodness-of-fit on F2	1.148	1.085	1.095	1.078	1.053	1.085
Final R indices [I>2sigma(I)]						
R1	0.0185	0.0154	0.0172	0.0204	0.0171	0.0157
wR2	0.0552	0.041	0.0454	0.0517	0.0483	0.0411
R indices (all data)						
R1	0.0185	0.0155	0.0175	0.0211	0.0178	0.016
wR2	0.0553	0.0411	0.0455	0.0521	0.0489	0.0414
Largest diff. e $Å^{-3}$						
peak	0.361	0.315	0.372	0.590	0.787	0.472
hole	-1.913	-0.956	-1.092	-1.032	-0.366	-0.425

Note: 5.1° to 61.0° 2Θ range, temperature 100 K, space group R3c. Parenthetical values are standard deviations.

Figures

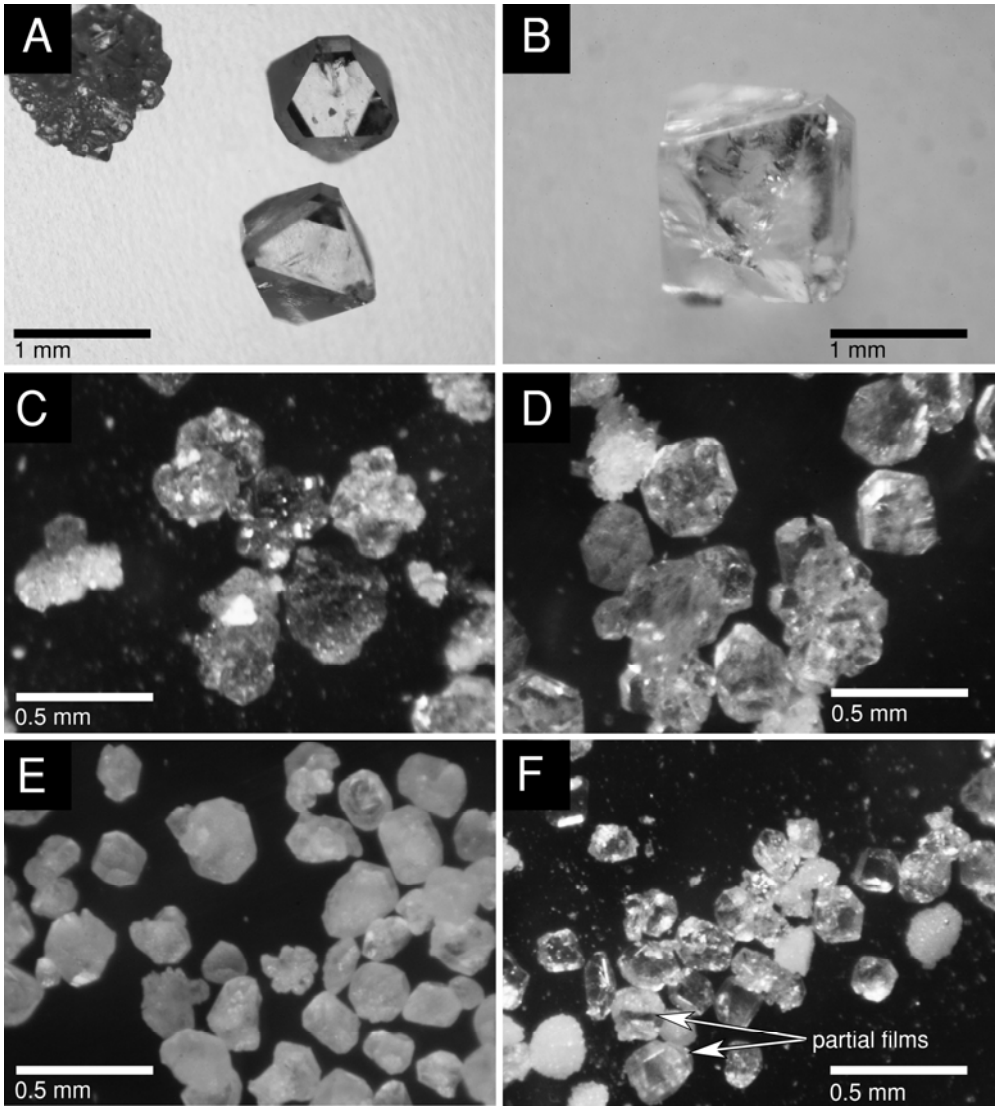

Figure 1.

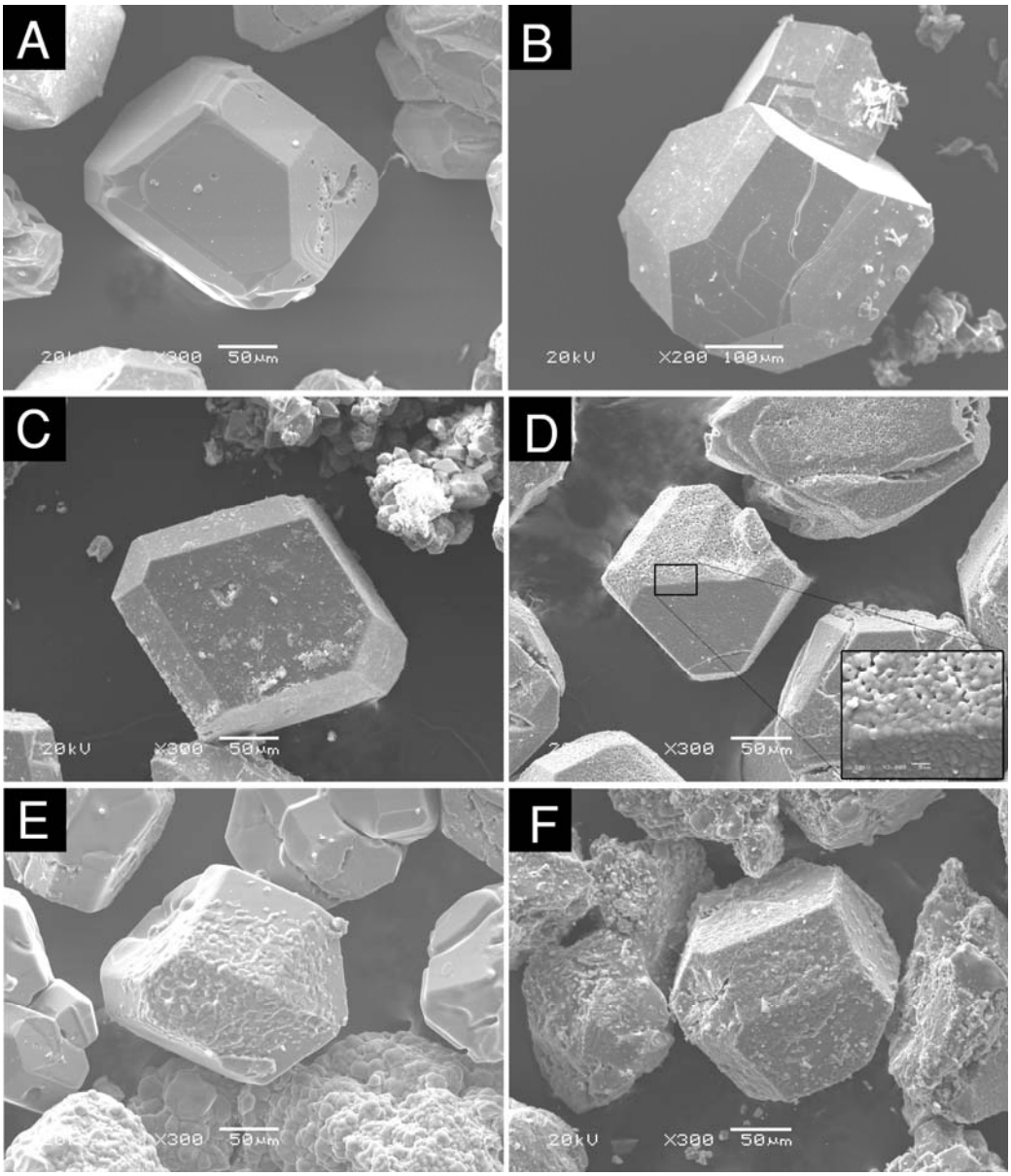

Figure 2.

849

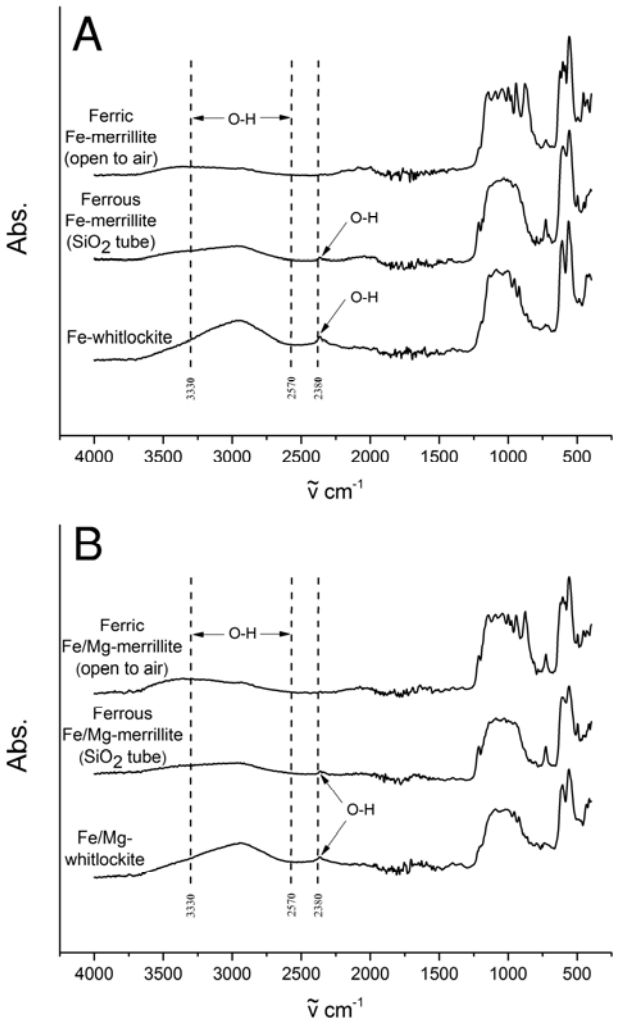

850

851 **Figure 3.**

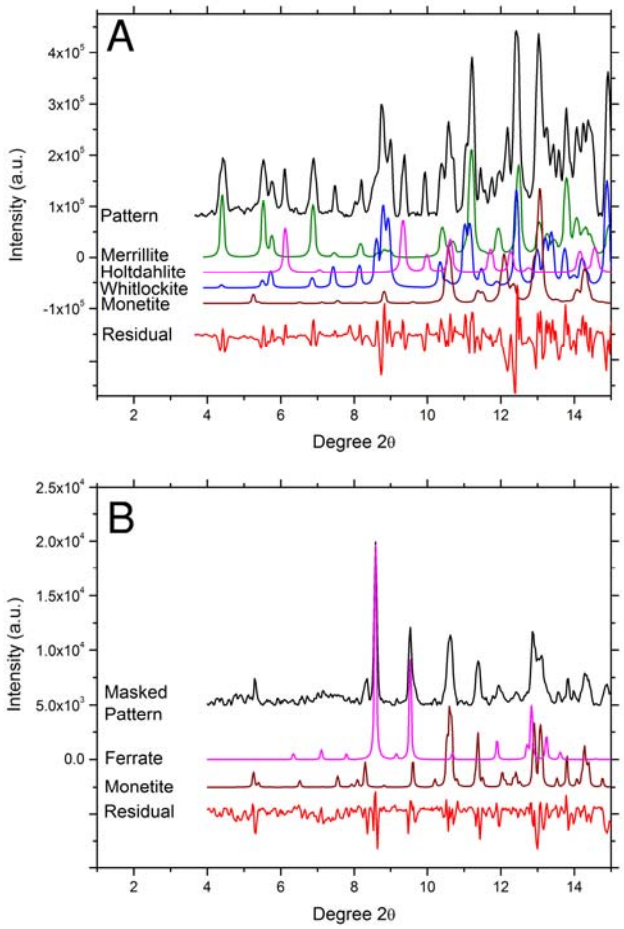

852
853 **Figure 4.**